engineering proceedings

MDPI

Proceeding Paper

Synthesis, Characterization, and Photocatalytic Activity of Sb_2O_3 Nanoparticles: A Step towards Environmental Sustainability †

Sabeeha Jabeen [1,2], Ekhlakh Veg [1,3], Shashi Bala [2] and Tahmeena Khan [1,*]

[1] Department of Chemistry, Integral University, Lucknow 226026, Uttar Pradesh, India; jsabeeha@student.iul.ac.in (S.J.); akhlakh@student.iul.ac.in (E.V.)
[2] Department of Chemistry, University of Lucknow, Lucknow 226007, Uttar Pradesh, India; shashichem15@gmail.com
[3] Department of Chemistry, Isabella Thoburn College, Lucknow 226007, Uttar Pradesh, India
* Correspondence: tahmeenak@iul.ac.in
† Presented at the 3rd International Electronic Conference on Processes—Green and Sustainable Process Engineering and Process Systems Engineering (ECP 2024), 29–31 May 2024; Available online: https://sciforum.net/event/ECP2024.

Abstract: Various nano-photocatalysts have been used to decompose organic dyes. Sb_2O_3 nanoparticles (NPs) have emerged as potential photocatalysts due to their redox potential, non-toxicity, long-term stability, and low cost. This work describes the fabrication of Sb_2O_3 NPs via the solvothermal process. A field emission scanning electron microscopic (FE-SEM) analysis depicted the spherical shape of the NPs, and an energy-dispersive X-ray (EDAX) analysis confirmed the presence of oxygen (O) and antimony (Sb) in the synthesized NPs. XRD (X-ray diffraction) patterns were recorded to measure the size and phase of the NPs. The sample was found with an alpha phase of antimony oxide indicating high purity. The Scherrer equation was used to calculate the size of the NPs, which was found to be approximately 20.89 nm. The photocatalytic potential was tested against methylene blue (MB) dye. The NPs showed a 60% degradation of the dye in 60 min. The dye was found to be adsorbed on the Sb_2O_3 nanoball surface and degradation was associated with the generation of reactive oxygen species (ROS).

Keywords: methylene blue dye; photocatalysis; Sb_2O_3; solvothermal synthesis

Citation: Jabeen, S.; Veg, E.; Bala, S.; Khan, T. Synthesis, Characterization, and Photocatalytic Activity of Sb_2O_3 Nanoparticles: A Step towards Environmental Sustainability. *Eng. Proc.* **2024**, *67*, 8. https://doi.org/10.3390/engproc2024067008

Academic Editor: Giancarlo Cravotto

Published: 31 July 2024

1. Introduction

Sb_2O_3 NPs have been proposed as a promising resolution for wastewater treatment [1]. High surface-to-volume ratios of the NPs facilitate the interaction between them and the pollutants leading to their active adsorption and catalytic degradation [2]. Antimony oxides are an important class of compounds having three different phases viz. antimony trioxide (Sb_2O_3), antimony tetroxide (Sb_2O_4), and antimony pentoxide (Sb_2O_5). Changes in Gibbs energy affect the formation of the desired phase [3,4]. Sb_2O_3 NPs also have good properties such as a higher refractive index [5], wear resistance, higher conductivity [6], excellent mechanical properties, and higher absorbing power [7]. Sb_2O_3 NPs have excellent chemical stability, energy consumption, and thermal performance, making them appropriate for wastewater remediation [8] as they can eradicate numerous pollutants from wastewater, together with heavy metals, chemicals, and dyes. The surface of the NPs can be altered to enhance their adsorption capacity and selectivity for pollutants [9]. Furthermore, Sb_2O_3 NPs are easy to recover and recycle, cost-effective for large-scale wastewater treatment, and can be utilized as nano photocatalysts in advanced oxidation processes (AOPs) to produce hydroxyl radicals in the presence of light [10]. The optical properties of the Sb_2O_3 NPs, such as energy diffraction and energy absorption of light, make the photocatalysis of many organic compounds more effective [11,12]. The antibacterial properties of the Sb_2O_3 NPs have also been explored [13]. They inhibit the growth of bacteria and other organisms

in wastewater, thereby reducing the risk of waterborne diseases [14]. According to the previous literature, Sb_2O_3 NPs synthesized via the hydrothermal route showed excellent potential for the degradation of Malachite green dye (MG) [15]. In another study, Sb_2O_3 NPs with different morphologies demonstrated superhydrophobic properties and excellent anticorrosion properties [16]. Furthermore, the photocatalytic degradation of Rhodamine B using the valentinite Sb_2O_3 NPs was also reported previously [17]. In this work, the authors have reported the synthesis and characterization of Sb_2O_3 NPs via the solvothermal process, and the photocatalytic efficiency of the NPs was evaluated against MB dye, which is associated with potential toxicity when used in high concentrations or administered incorrectly. Swallowing or injecting the dye can cause serious side effects, including methemoglobinemia, a condition in which the blood's ability to carry oxygen is impaired. In addition, its prolonged exposure can cause skin irritation and allergies. Another problem is that it can smudge and discolor, which can be a problem when dealing with soft products or in some applications where true color representation is important [18,19].

2. Materials and Methods

Antimony chloride ($SbCl_3$) and methylene blue dye were procured from Sigma Aldrich, (St. Louis, MO, USA) and ammonium hydroxide (NH_4OH) was procured from MERCK India (MITC), Tower 3 (Bengaluru, Karnataka, India). FT-IR spectrum was recorded on a Bruker Tensor instrument in the scanning range of 4000–400 cm^{-1} through the KBr pellet method. The X-ray crystallographic study was performed on a Rigaku Ultima IV diffractometer, in Tokyo, Japan, to measure the particle size. UV–Vis spectra were recorded on a Hitachi U3900 spectrometer to assess the absorbance frequency and Tauc plot for bandgap measurement. The crystal structure and purity of the Sb_2O_3 NPs were measured through a diffractometer (XRD, Rigaku Ultima IV, Tokyo, Japan). The structure of the NPs was determined using a scanning electron microscope (SEM) Zeiss Gemini SEM 500 with EDAX detector, Singapore) FESEM Analyzer Zeiss Gemini SEM 50 with an acceleration voltage of 0.02–30 kV and with thermal field emission type, probe current pA of 20 nA, and a magnification of 50×—2,000,000×. An EDAX analysis of the samples was carried out on a Bruker energy-dispersive X-ray spectrometer. All chemicals were of analytical reagent (AR) grade and used without additional refinement.

Synthesis of Sb_2O_3 NPs

114 mg (0.1 M) of $SbCl_3$ was dissolved into 50 mL of ethanol. A freshly prepared 6 mL of 10 mol/L NH_4OH was added to it with constant stirring for 60 min to maintain pH at 10 and was then shifted to an autoclave [20]. The autoclave was set at 120–160 °C for 10 h and cooled to room temperature. The resultant white powder was washed with distilled water, followed by ethanol to remove impurities, and then dried at 60 °C for 3 h [21]. The alcoholysis of $SbCl_3$ is depicted in Equations (1)–(3), in which R group denotes hydrocarbyl [22].

$$SbCl_3 + 3ROH \rightarrow Sb(OR)_3 + 3HCl \quad (1)$$

$$Sb(OR)_3 + 4OH^- \rightarrow Sb(OH)_4{}^- + 3RO^- \quad (2)$$

$$Sb(OH)_4{}^- \rightarrow Sb_2O_3 + 3OH^- + 3H_2O \quad (3)$$

3. Results and Discussion

3.1. Characterization Tactics

3.1.1. XRD

To evaluate the crystalline size and phase of Sb_2O_3 NPs, the XRD patterns were recorded (Figure 1). Using the JCPDS data card (card number 05-0534), with a preferred plane of (222), the sample was found with an alpha phase of Sb_2O_3 NPs, indicating high purity [23]. The average crystallite size (D) was calculated through the Scherrer Equation (4) [24].

$$D = k\lambda / \beta \cos\theta \quad (4)$$

where k = Scherrer constant (0.94);
λ = Wavelength of the incident X-ray (1.542 Å);
β = Full width at half maximum (FWHM) of the diffraction peak;
θ = Angle of diffraction.

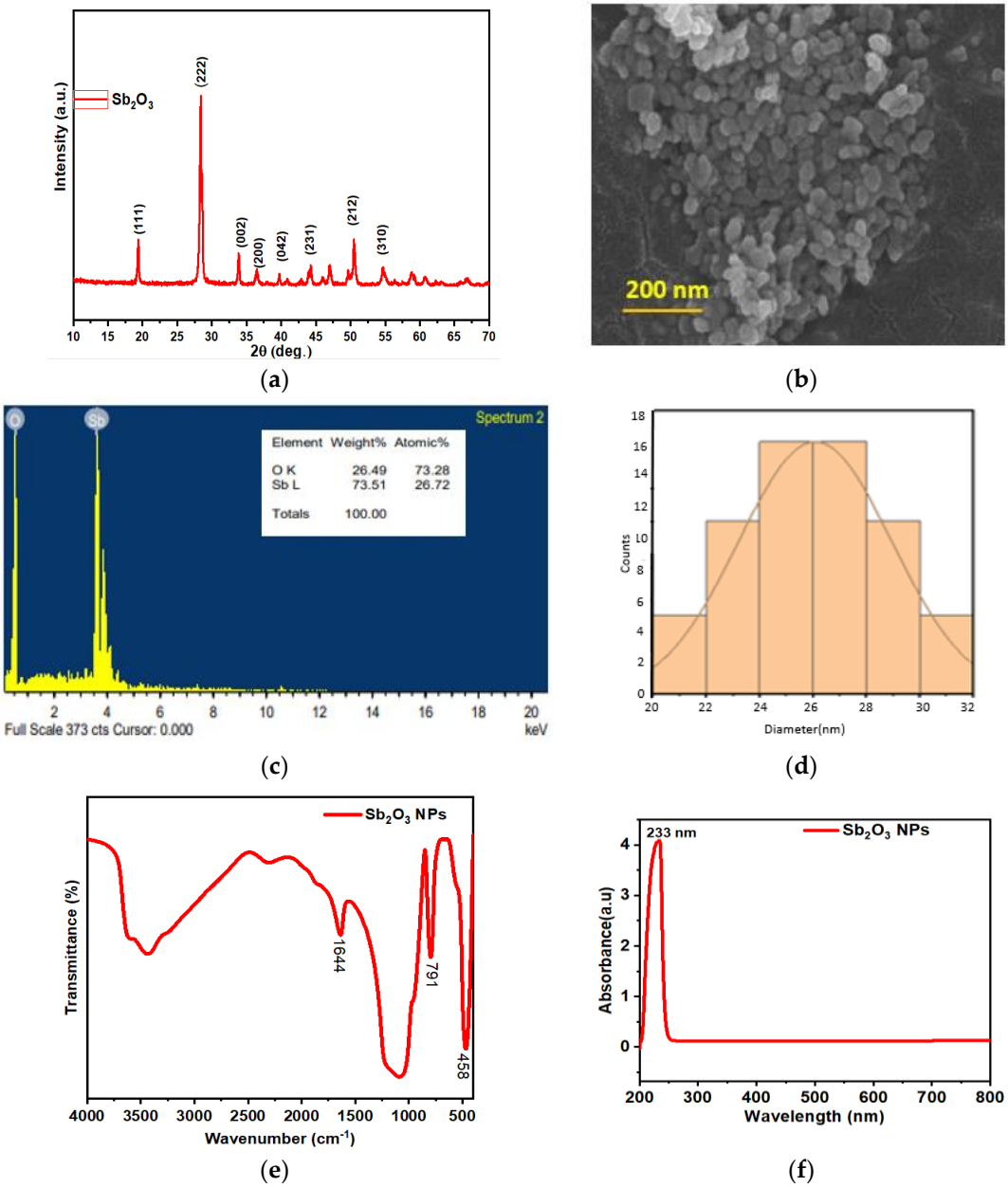

Figure 1. (**a**) XRD spectrum, (**b**) SEM image, (**c**) EDAX spectrum, (**d**) average particle size, (**e**) FT-IR spectrum, and (**f**) UV-Vis spectrum of Sb_2O_3 NPs.

The average grain size was calculated to be 20.89 nm, as demonstrated in Table 1.

Table 1. XRD data and calculation of the average size.

Material	2θ Value	FWHM Value	Crystallite Size at Different θ Values (nm)	Average Crystallite Size of Sb_2O_3 NPs (nm)
Sb_2O_3 NPs	19.29°	0.43	20.91	20.89 nm
	28.36°	0.41	20.87	

3.1.2. SEM Analysis

The synthesized NPs showed distinct particles with no agglomeration. Figure 1b reveals the spherical morphology of the Sb_2O_3 NPs [25,26]. Figure 1c shows the EDAX spectrum, confirming the presence of O and Sb. The particle size was calculated using Figure 1d, showing an average particle size of 26 nm.

3.1.3. FT-IR Analysis

The absorption bands at 458 cm^{-1} and 791 cm^{-1} demonstrated the stretching frequencies (Sb-O), oxide bridge functional group (O-Sb-O), and symmetric and asymmetric vibration of Sb_2O_3. The peak at 1644 cm^{-1} was attributed to the bending vibrations of H_2O [15,27]. The lesser intensity of the peak showed a low content of humidity in the as-prepared sample.

3.1.4. UV-Vis Analysis

Figure 1f depicts the UV-Vis absorption spectrum of Sb_2O_3 NPs. The maximum absorbance was obtained at 233 nm. In a previous study, the optical absorption spectrum of the Sb_2O_3 NPs showed an absorption peak around 298 nm [28]. The bandgap energy was obtained using Tauc's Equation (5):

$$h\nu \cdot \alpha = (Ah\nu - Eg)\, n/2 \tag{5}$$

where Eg is the optical bandgap, ν is the frequency of light, and A is a constant for the direct transition value of $n = 1$ and indirect transition, $n = 2$—from the plot of (F(R) × $h\nu$) 1/2 versus $h\nu$. The estimated bandgap value for Sb_2O_3 NPs was found to be 3.32 eV, which was almost similar to the previously reported literature [29].

3.2. Photocatalytic Potential of Sb_2O_3 NPs

The photocatalytic activity was investigated against MB dye in aqueous media under UV light illumination. A dye solution with an initial concentration of C_0 was prepared, and an appropriate amount of Sb_2O_3 NPs was added to it in separate beakers. Before irradiation, the samples were agitated for 20 min in the dark to check the adsorption/desorption equilibrium. In all the settings in the dark, the dye concentration did not change, suggesting very little or insignificant adsorption. Then, the reaction chamber was irradiated with UV light to form photoexcited charge carriers (electron (e^-) and hole (h^+); the photocatalytic potential was tested against MB dye at room temperature in the presence of UV light. A total of 40 mg of Sb_2O_3 nanoballs was distributed in 100 mL (10 ppm) of MB dye solution; 5 mL solution was collected at an interval of 20 min from the prepared sample for the UV-Vis analysis. Then, 60% dye was degraded in 60 min as depicted in Figure 2a,b, which depicts the kinetics of the dye degradation. The dye degradation percentage was calculated using Equation (6) [30,31].

$$\text{Percentage of degradation} = \frac{C_0 - C_t}{C_0} \times 100 \tag{6}$$

The kinetics of photodegradation were also studied using the Langmuir–Hinshelwood model as Equation (7):

$$ln\left[\frac{C_0}{C_t}\right] = K_{app}t \tag{7}$$

where C_0 and C_t represent the dye concentrations at the time '0' and 't', respectively, and 'K_{app}' represents the apparent pseudo-first-order rate constant. The maximum photodegradation rate (0.70 min^{-1}) with excellent linear correlation was demonstrated by the Sb_2O_3 NPs, suggesting pseudo-first-order kinetics as depicted in Figure 2b.

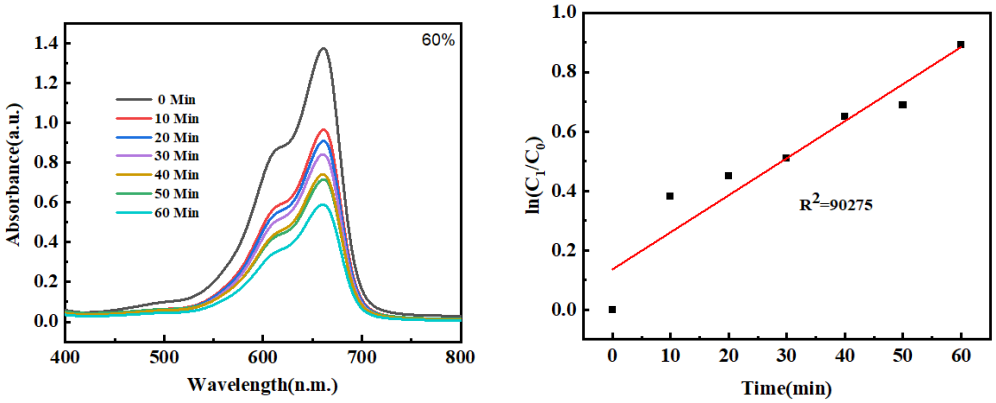

(**a**) (**b**)

Figure 2. (**a**) Photodegradation of MB dye; (**b**) kinetics of dye degradation.

The probable mechanism of MB degradation is depicted in Figure 3a. The increase in MB adsorption on the Sb_2O_3 NP surface may react with ROS during the photocatalytic process. When a photon with hν energy from a visible light source collides with the surface of synthesized nanostructures, an electron (e^-) in the valence band (VB) becomes excited and jumps to the conduction band (CB), leaving a hole (h^+) in the valence band (Equation (8)) and electrons of the conduction band produce superoxide (Equation (9)). The reaction between superoxide and water generates hydroxyl radicals (Equation (10)) [32]. It can also interact with hydroxyl groups in water to form OH radicals (Equation (11)) [33,34]. The hydroxyl radical reacts with the dye, reducing the dye to CO_2 and H_2O (Equation (12)).

$$Sb_2O_3 + h\nu \rightarrow Sb_2O_3\ (e^-{}_{CB} + h^+{}_{VB}) \quad (8)$$

$$e^-{}_{CB} + O_2 \rightarrow O_2{}^{\bullet -} \quad (9)$$

$$O_2{}^{\bullet -} + H_2O \rightarrow {}^{\bullet}OH + {}^{-}OH + O_2 \quad (10)$$

$$h^+{}_{VB} + H_2O \rightarrow {}^{\bullet}OH \quad (11)$$

$$Reactive\ species\ ({}^{\bullet}OH, O_2{}^{\bullet -}) + Dye\ (organic\ pollutant) \rightarrow Degradation\ products \quad (12)$$

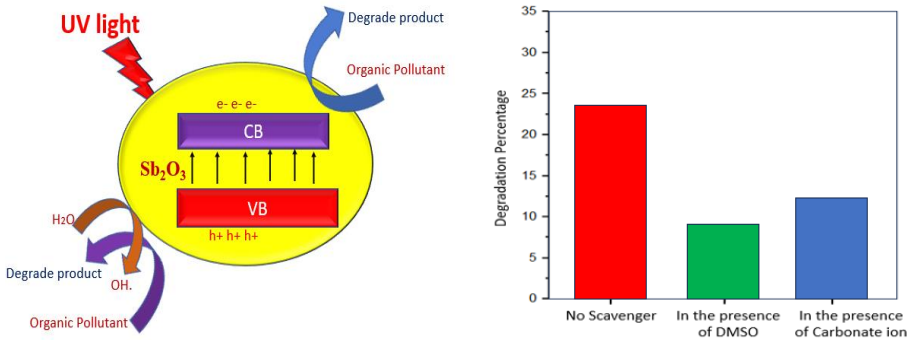

(**a**) (**b**)

Figure 3. (**a**) Proposed mechanism of photocatalysis; (**b**) quenching experiments.

3.3. Quenching Experiment

To study the qualitative effect, DMSO and carbonate ions have been used as scavengers for chemically active species. To carry out the experiment, the concentration of Sb_2O_3 NPs taken was 0.5 g/L and the concentration of DMSO or carbonate ions taken was 0.4 g/L in 100 mL of dye solution. The reaction mixture was irradiated via UV–visible radiation for 60 min. It was observed that in the absence of a scavenger (DMSO or carbonate ion), the percentage degradation of dye was 27.5%, but when DMSO or a carbonate ion was

added to the dye solution, the percentage degradation of the dye decreased to 10.3 and 13.5%, respectively (Figure 3b). From the experimental results, it was concluded that the concentration of active radicals which are responsible for the degradation decreased in the presence of scavengers [35]. The scavenging mechanism is shown in Equations (13) and (14):

$$OH^{\bullet} + (CH_3)_2SO \rightarrow CH_3^{\bullet} + CH_3SO_2H \quad (13)$$

$$OH^{\bullet} + CO_3^{2-} \rightarrow OH^{-} + CO_3^{-} \quad (14)$$

4. Conclusions

The fabrication of Sb_2O_3 NPs has been effectively achieved via the solvothermal process and has shown excellent adsorption and photocatalytic activity towards MB dye. The photocatalytic activity of Sb_2O_3 NPs is increased in UV light exposure, which is attributed to the recombination of photogenerated electrons and holes and the generation of more reactive oxygen species. The photocatalyst followed Langmuir and Freundlich's adsorption isotherm and the maximum photocatalytic activity was found to be 60.2%. The correlation coefficient value (R^2 = 0.90278) showed the rate followed by pseudo-first-order kinetics. Owing to excellent adsorption capacity, surface area, and photocatalytic activity, Sb_2O_3 NPs have shown a dual role in the removal of MB dye. With the obtained results, it can be concluded that the photocatalyst can be used for practical implementation in industries for the treatment of wastewater.

Author Contributions: Investigation, formal analysis and writing-original draft, S.J.; writing-final draft, E.V.; resources, S.B.; Conceptualization and Supervision, T.K. All authors have read and agreed to the published version of the manuscript.

Funding: This research received no external funding.

Institutional Review Board Statement: Not applicable.

Informed Consent Statement: Not applicable.

Data Availability Statement: No new data were generated during the study.

Acknowledgments: The authors are thankful to the R&D cell of the University for providing the Manuscript Communication Number (IU/R&D/2023-MCN0002061). The authors are also thankful to Anil Mishra, Head of the Department of Chemistry at Lucknow University, for providing the necessary requisite laboratory facilities and the USIF, Aligarh Muslim University, Aligarh, for providing analytical and microscopic facilities. They are also thankful to Abdul Rahman Khan, Head of the Department of Chemistry at Integral University, Lucknow for the necessary support.

Conflicts of Interest: The authors declare no conflicts of interest.

References

1. Jabeen, S.; Ahmad, N.; Bala, S.; Bano, D.; Khan, T. Nanotechnology in environmental sustainability and performance of nanomaterials in recalcitrant removal from contaminated Water: A review. *Int. J. Nano Dimens.* **2023**, *14*, 1–28.
2. Wang, Z.; Deb, A.; Srivastava, V.; Iftekhar, S.; Ambat, I.; Sillanpää, M. Investigation of textural properties and photocatalytic activity of PbO/TiO_2 and Sb_2O_3/TiO_2 towards the photocatalytic degradation Benzophenone-3 UV filter. *Sep. Purif. Technol.* **2019**, *228*, 115763. [CrossRef]
3. Wilde, G. Structural phase transformations in nanoscale systems. *Adv. Eng. Mater.* **2021**, *23*, 2001387. [CrossRef]
4. Jagannath, G.; Eraiah, B.; Gaddam, A.; Fernandes, H.; Brazete, D.; Jayanthi, K.; Krishnakanth, K.N.; Venugopal Rao, S.; Ferreira, J.M.; Annapurna, K.; et al. Structural and femtosecond third-order nonlinear optical properties of sodium borate oxide glasses: Effect of antimony. *J. Phys. Chem. C* **2019**, *123*, 5591–5602. [CrossRef]
5. Zhang, X.; Lu, C.; Geng, M.; Xu, K.; Zong, S. Effects of surface area on all-solid-stated pH sensor based on antimony electrode. *IEEE Sens. J.* **2019**, *20*, 680–688. [CrossRef]
6. Chin, H.S.; Cheong, K.Y.; Razak, K.A. Review on oxides of antimony nanoparticles: Synthesis, properties, and applications. *J. Mater. Sci.* **2010**, *45*, 5993–6008. [CrossRef]
7. Zia, J.; Riaz, U. Photocatalytic degradation of anti-inflammatory drug using POPD/ Sb_2O_3 organic-inorganic nanohybrid under solar light. *J. Mater. Res. Technol.* **2019**, *8*, 4079–4093. [CrossRef]

8. Barik, P.; Bhattacharjee, A. The Integral Postulation of Inorganic Nanofiller-Derived Polymer Applications in Agriculture. In *Nanofillers*; CRC Press: Boca Raton, FL, USA, 2023; pp. 221–257.
9. Pu, Y.; Zhao, F.; Chen, Y.; Lin, X.; Yin, H.; Tang, X. Enhanced Electrocatalytic Oxidation of Phenol by Sn_2O_2-Sb_2O_3 /GAC Particle Electrodes in a Three-Dimensional Electrochemical Oxidation System. *Water* **2023**, *15*, 1844. [CrossRef]
10. Zhu, L.J.; Xue, H.; Xiao, L.R.; Chen, Q.H. Preparation and photocatalytic performance of cubic Sb_2O_3 nanocrystalline. *Chin. J. Inorg. Chem.* **2012**, *28*, 2165–2169.
11. Sato, J.; Saito, N.; Nishiyama, H.; Inoue, Y. Photocatalytic water decomposition by RuO_2-loaded antimonates, $M_2Sb_2O_3$ (M=Ca, Sr), $CaSb_2O_6$ and $NaSbO_3$, with d10 configuration. *J. Photochem. Photobiol. A Chem.* **2002**, *148*, 85–89. [CrossRef]
12. Liu, W.J.; Lin, P.Y.; Jin, H.; Xue, H.; Zhang, Y.F.; Li, Z.H. Nanocrystalline $ZnSb_2O_6$ hydrothermal synthesis, electronic structure, and photocatalytic activity. *J. Mol. Catal. A Chem.* **2011**, *349*, 80–85. [CrossRef]
13. Fu, Y.H.; Xue, H.; Qin, M.; Liu, P.; Fu, X.Z.; Li, Z.H. Nanocrystalline $GaSbO_4$ with high surface area prepared via a facile hydrothermal method and its photocatalytic activity study. *J. Alloys Compd.* **2012**, *522*, 144–148. [CrossRef]
14. Li, F.; Cheng, L.; Fan, J.; Xiang, Q. Steering the behavior of photogenerated carriers in semiconductor photocatalysts: A new insight and perspective. *J. Mater. Chem. A* **2021**, *9*, 23765–23782. [CrossRef]
15. Jabeen, S.; Ganie, A.S.; Ahmad, N.; Hijazi, S.; Bala, S.; Bano, D.; Khan, T. Fabrication and studies of $LaFe_2O_3$/Sb_2O_3 heterojunction for enhanced degradation of Malachite green dye under visible light irradiation. *Inorg. Chem. Commun.* **2023**, *152*, 110729. [CrossRef]
16. Zhu, S.; Yang, X.; Li, T.; Li, F.; Cao, W. Phase and morphology controllable synthesis of superhydrophobic Sb_2O_3 via a solvothermal method. *J. Alloys Compd.* **2017**, *721*, 149–156. [CrossRef]
17. Abdellatif, M.; Louafi, Y.; Nunes, D.; Freire, T.; Fortunato, E.; Martins, R.; Kabouche, S.; Trari, M. Studies on photocatalytic degradation of Rhodamine B using the valentinite Sb_2O_3. *React. Kinet. Mech. Catal.* **2023**, *136*, 1643–1655. [CrossRef]
18. Khan, I.; Saeed, K.; Zekker, I.; Zhang, B.; Hendi, A.H.; Ahmad, A.; Ahmad, S.; Zada, N.; Ahmad, H.; Shah, L.A.; et al. Review on Methylene Blue: Its Properties, Uses, Toxicity and Photodegradation. *Water* **2022**, *14*, 242. [CrossRef]
19. Kumari, H.; Sonia Suman Ranga, R.; Chahal, S.; Devi, S.; Sharma, S.; Kumar, S.; Kumar, P.; Kumar, S.; Kumar, A. A Review on Photocatalysis Used For Wastewater Treatment: Dye Degradation. *Water Air Soil Pollut.* **2023**, *234*, 349. [CrossRef]
20. Li, M.; Zhu, L.; Liu, X.; Yu, Y.; Zhang, H.; Yu, B.; Chen, B.H. Synthesis of Antimony Trioxide Crystals with Various Morphologies and Their UV-Vis-NIR Reflectance Performance. *ChemistrySelect* **2018**, *3*, 4310–4314. [CrossRef]
21. Qi, W.; Guo, S.; Sun, H.; Liu, Q.; Hu, H.; Liu, P.; Zhang, M. Synthesis and characterization of Sb_2O_3 nanoparticles by liquid phase method under acidic conditions. *J. Cryst. Growth* **2022**, *588*, 126642. [CrossRef]
22. Makhloufi, R.; Hachani, S.E.; Zekri, Z.; Tair, W. Solvothermal Synthesis of Antimony Trioxide Sb_2O_3 Used as a Photocatalyst for Crystal Violet Dye Degradation. *Mosc. Univ. Chem. Bull.* **2022**, *77*, 111–116. [CrossRef]
23. Shan, C.W.; Hu, H.T.; Chen, Z.; Han, G.C.; Feng, X.Z.; Kraatz, H.B. Fabrication of block-shaped Sb_2O_3 and flower-shaped CoNPs nanocomposites for ultrasensitive antioxidant quercetin sensing and its electrooxidation mechanism. *Microchem. J.* **2024**, *201*, 110661. [CrossRef]
24. Jabeen, S.; Siddiqui, V.U.; Bala, S.; Mishra, N.; Mishra, A.; Lawrence, R.; Bansal, P.; Khan, A.R.; Khan, T. Biogenic Synthesis of Copper Oxide Nanoparticles from Aloe vera: Antibacterial Activity, Molecular Docking, and Photocatalytic Dye Degradation. *ACS Omega* **2024**, *9*, 30190–30204. [CrossRef]
25. Tan, Y.M.; Chen, X.H.; Zhu, Y.R.; Chen, L.J. Synthesis of spherical tremella-like Sb_2O_3 structures derived from the metal-organic framework and its lithium storage properties. *J. Cent. South. Univ.* **2019**, *26*, 1469–1480. [CrossRef]
26. Bai, H.; Guo, H.; Wang, J.; Dong, Y.; Liu, B.; Guo, F.; Zheng, Y. Hydrogen gas sensor based on SnO_2 nanospheres modified with Sb_2O_3 prepared by the one-step solvothermal route. *Sens. Actuators B Chem.* **2021**, *331*, 129441. [CrossRef]
27. Ersundu, A.E.; Çelikbilek, M.; Baazouzi, M.; Soltani, M.T.; Troles, J.; Aydin, S. Characterization of new Sb_2O_3-based multicomponent heavy metal oxide glasses. *J. Alloys Compd.* **2014**, *615*, 712–718. [CrossRef]
28. Ochirkhuyag, A.; Tóth, I.Y.; Kormányos, A.; Janáky, C.; Kónya, Z. Composition-Dependent Optical and Photoelectrochemical Behavior of Antimony Oxide Iodides. *J. Electrochem. Soc.* **2019**, *166*, H3202. [CrossRef]
29. Divya, K.V.; Abraham, K.E. Ag nanoparticle decorated Sb_2O_3 thin film: Synthesis, characterizations and application. *Nano Express* **2020**, *1*, 020005. [CrossRef]
30. Rosaline, D.R.; Suganthi, A.; Vinodhkumar, G.; Inbanathan, S.S.R.; Umar, A.; Ameen, S.; LuizFoletto, E. Enhanced sunlight-driven photocatalytic activity of SnO_2- Sb_2O_3 composite towards emerging contaminant degradation in water. *J. Alloys Compd.* **2022**, *897*, 162935. [CrossRef]
31. He, G.H.; Liang, C.J.; Ou, Y.D.; Liu, D.N.; Fang, Y.P.; Xu, Y.H. Preparation of novel Sb_2O_3/WO_3 photocatalysts and their activities under visible light irradiation. *Mater. Res. Bull.* **2013**, *48*, 2244–2249. [CrossRef]
32. Wang, Z.; Srivastava, V.; Iftekhar, S.; Ambat, I.; Sillanpää, M. Fabrication of Sb_2O_3/PbO photocatalyst for the UV/PMS-assisted degradation of carbamazepine from synthetic wastewater. *Chem. Eng. J.* **2018**, *354*, 663–671. [CrossRef]
33. Jabeen, S.; Ganie, A.S.; Bala, S.; Khan, T. Photocatalytic Degradation of Malachite Green Dye via An Inner Transition Metal Oxide-Based Nanostructure Fabricated through a Hydrothermal Route. *Mater. Proc.* **2023**, *14*, 5. [CrossRef]

34. Khan, I.; Saeed, K.; Ali, N.; Khan, I.; Zhang, B.; Sadiq, M. Heterogeneous photodegradation of industrial dyes: An insight to different mechanisms and rate affecting parameters. *J. Environ. Chem. Eng.* **2020**, *8*, 104364. [CrossRef]
35. Jabeen, S.; Siddiqui, V.U.; Sharma, S.; Rai, S.; Bansal, P.; Bala, S.; Raza, A.; Ahmad, M.I.; Khan, A.R.; Khan, T. A novel green synthesis of $CuFe_2O_4$ Nanoparticles from Cissus rotundifolia for photocatalytic and antimicrobial activity evaluation. *J. Alloys Compd.* **2024**, *984*, 174020. [CrossRef]